Int. J. Microgravity Sci. Appl., **36** (3) (2019) 360303
DOI: 10.15011//jasma.36.360303

IIII Original Paper IIII

Temperature-Field Analysis of Flame Spread over Droplet-Cloud Elements with Interactive Droplets in Microgravity aboard Kibo on ISS

Yasuko YOSHIDA [1], Takehiko SEO [1], Masato MIKAMI [1] and Masao KIKUCHI [2]

Abstract

Liquid-fuel combustion experiments titled “Elucidation of Flame Spread and Group Combustion Excitation Mechanism of Randomly Distributed Droplet Clouds (Group Combustion)” were conducted in 2017 as the first of the combustion experiments in the Japanese Experimental Module “Kibo” aboard the International Space Station (ISS). This paper reports temperature-field analysis by the TFP method based on visible light emissions for the flame spread of droplet-cloud elements composed of four droplets with two or three interactive droplets, which was conducted as part of the “Group Combustion” experiments. The results show that the position of the interactive droplets affects the flame spread around the droplets, and the flame-spread limit is extended by the interactive effect. If a burning droplet pre-heats a droplet existing outside the flame-spread limit, the pre-vaporization also extends the flame-spread limit around two interactive droplets.

Keyword(s): Droplet combustion, Flame spread, Droplet cloud, Microgravity.
Received 13 May 2019, Accepted 23 July 2019, Published 31 July 2019.

1. Introduction

Liquid-fuel combustion experiments titled “Elucidation of Flame Spread and Group Combustion Excitation Mechanism of Randomly Distributed Droplet Clouds (Group Combustion)” [1)] was conducted from February to July in 2017 as the first of the combustion experiments in the Japanese Experimental Module “Kibo” aboard the International Space Station (ISS). The purpose of the “Group Combustion” experiments is to study hypotheses about local flame-spread rules using droplet-cloud elements and droplet arrays and the flame-spreading behavior of randomly distributed droplet clouds on the effects of interaction in the long duration microgravity aboard "Kibo" [2)]. Yoshida et al.[3)] conducted flame-spread experiments on droplet-cloud elements consisting of four droplets and investigated the flame-spread-limit distribution around droplet-cloud elements with two or three interactive burning droplets. Mikami et al.[2)] conducted experiments on randomly distributed droplet clouds consisting of a large number of droplets and investigated the overall flame spread characteristics under conditions where the mean droplet spacing was changed.

This study is an extension of the research by Yoshida et al.[3)] on the flame-spread over droplet-cloud elements and includes temperature-field analysis using the Thin Filament Pyrometry (TFP) method based on visible light emissions from SiC fibers tethering droplet-cloud elements to study the effect of droplet interaction. We investigated the influence of the position of the interactive droplets on the flame spread considering the temporal variation of the iso-thermal line distribution.

2. Experimental Apparatus and Conditions

This research conducted flame-spread experiments using the experimental device Group Combustion Experiment Module (GCEM) [4)] in microgravity aboard Kibo on ISS. A droplet-cloud-generation device and ignition device were installed in an aluminum combustion vessel with a volume of 13 L. The flame spread was observed from outside the combustion chamber by a digital video camera (Canon, EOS 5D Mark II) through a window made of sapphire glass.

Figure 1 shows the droplet-cloud-element model and the droplet support unit with a SiC-fiber lattice and the ignition unit[4)]. The droplets were generated one by one to form a droplet cloud at the designated intersection of a 30×30 lattice with 14-μm SiC fibers (Nihon Carbon, Hi-Nicalon) stretched at 4-mm intervals. The fuel was n-decane. A predetermined amount of fuel was pushed out from a syringe unit driven by a stepping motor through a Teflon tube, and the droplet was generated by supplying the fuel to an intersection of SiC fibers through a glass-tube needle whose tip was narrowed to an outer diameter of about 70 μm. An unevenly arranged droplet cloud was generated by repeating the droplet generation procedure while the position of the glass-tube needle was moved using a three-dimensional traverse device. A droplet near the center of one side of the SiC-fiber lattice was ignited by electrical heating of a Ni-Cr wire. As described by Mikami et al.[5)] and Farouk and Dryer[6)], the effect of a 14-μm SiC fiber on droplet combustion of 1 mm is negligible.

1 Yamaguchi University, 2-16-1 Tokiwadai, Ube, Yamaguchi 755-8611 Japan.
2 Japan Aerospace Exploration Agency, 2-1-1 Sengen Tsukuba, Ibaraki 305-8505, Japan.
(E-mail: w502wd@yamaguchi-u.ac.jp)

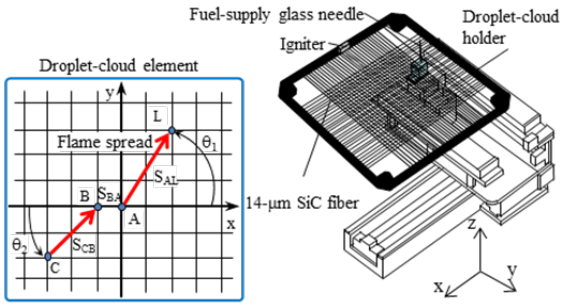

Fig. 1 Schematic of the droplet-cloud-element model and the droplet support unit with a SiC-fiber lattice and the ignition unit [3].

The droplet-cloud element shown in **Fig. 1** consists of four droplets: Droplet L to check the flame-spread limit from burning Droplet A, and Droplets B and C to check the droplet interaction with Droplet A. Droplet C was ignited by burning of Droplet I of 1 mm placed 12 mm away from Droplet C to start the flame spread of the droplet-cloud element. Droplet I, which is not shown in **Fig. 1**, did not affect the subsequent flame spread from Droplet C for d_0 of about 1 mm because Droplet I was far enough away from Droplet C as discussed by Oyagi et al.[7]. The position of Droplet L was varied to investigate the flame-spread limit from burning Droplet A to Droplet L. The spacing between Droplets A and L, S_{AL}, ranged from 12 to 24 mm. The direction angle θ_1 of Droplet L ranged from -90 deg. to 180 deg. The spacing between Droplets B and A was S_{BA}=4 mm. The spacing between Droplets C and B was S_{CB}=4, 11.3 and 12 mm. The direction angle θ_2 of Droplet C was 0, 45 and 90 deg. As mentioned above, d_0=1 mm was used in most cases. In the cases to investigate the flame-spread limit in detail, however, S_{AL}/d_0 was varied by changing d_0 from 0.92 mm to 1.15 mm for the same droplet spacing S_{AL}. The standard deviation of the initial droplet diameter d_0 of the same droplet-cloud element except for Droplet I was less than 4.5 %. Since we used a low-volatility fuel *n*-decane, the droplet diameter change from the start of the first droplet generation to ignition was less than 1 %. The local equivalence ratio in the gas phase at the droplet surface was 0.09 during the droplet generation process, which is much smaller than the lower flammability limit. Therefore, the pre-vaporization did not affect the flame spread significantly [8].

The temperature distribution around burning droplets was measured by the Thin Filament Pyrometry (TFP) method based on visible light emissions from 14-μm SiC fiber tethering droplets, according to the same method as that described by Mikami et al.[9]. The red value (R value) of pixels in the RGB image of the SiC fiber taken by a digital video camera was correlated with temperature measured by a 25-μm Pt-Pt/13%Rd thermocouple using a fitting function consideration of the temperature dependence of radiant energy density in Planck's radiation law. The present TFP method is valid for a narrow temperature range of 1100 K<T<1450 K with about 65-K accuracy.

3. Experimental results and discussion

Figure 2 shows typical sequential images of the flame spread behavior of droplet-cloud elements. Time t starts from the moment of ignition of Droplet A. We changed the brightness of each image from 0 % to 75 % and the contrast from 0 % to 40 % so that the visibility of blue flames is enhanced. The last image shows the image at the timing of Droplet L ignition. A bright blue flame is seen around Droplet L immediately after Droplet L ignition.

Figure 3 shows the flame-spread-limit distributions around burning Droplet A for S_{BA}/d_0 of about 4, where S_{CB}/d_0 is from about 4 to 12. The condition of the flame spreading to Droplet L is plotted as ○, the condition of no-flame spreading is plotted as ×. The flame-spread limit exists between ○ and ×. Both the horizontal axis and vertical axis are normalized by the average

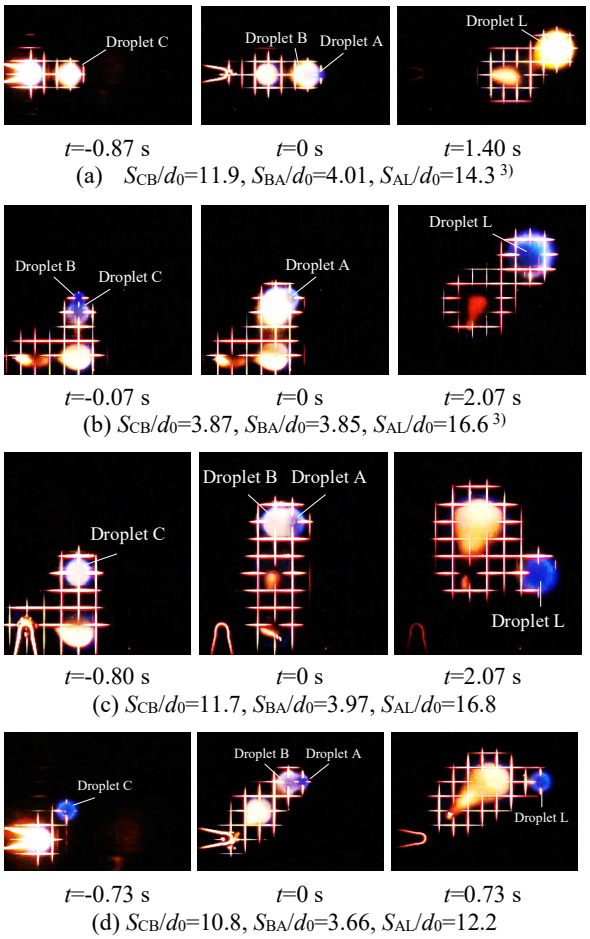

Fig. 2 Flame-spread behavior from Droplet C to Droplet L via Droplets B and A for different droplet arrangements.

initial droplet diameter d_0 of Droplets C, B, A and L. The flame-spread-limit distance $(S/d_0)_{limit}$ around a single droplet, FSL1, is shown as a chain line. The flame-spread-limit distance of a linear droplet array at room temperature and atmospheric pressure air is $(S/d_0)_{limit}=14$ [5] and is used as FSL1. The flame-spread-limit distance around an imaginary droplet with twice the volume located at the center of the mass of Droplets B and A, FSL2, is also shown as a dashed line. FSL2 is $2^{1/3}(S/d_0)_{limit}=17.6$ [9]. The flame-spread-limit distance around an imaginary droplet with three times the volume located at the center of the mass of Droplets C, B and A, FSL3, is shown as a two-dot chain line. FSL3 is $3^{1/3}(S/d_0)_{limit}=20.2$ [3].

In the case of **Fig. 3(a)**, the flame-spread limit exists outside FSL1 of Droplet A or Droplet B, almost coincides with FSL2 but is slightly inside FSL2 [3]. This clearly shows that two-droplet interactions enlarge the flame-spread limit. In the case of **Fig. 3(b)**, there exist some flame-spread conditions outside FSL2 of Droplets B and A for $0\leq\theta_1<45$ and FSL2 of Droplets C and B around $\theta_1=45$, and therefore the flame-spread limit exists between FSL2 and FSL3, showing the effect of three-droplet interaction under that condition. In the case of **Fig. 3(c)**, the data are plotted for the direction angle θ_1 of Droplet L from -45 to 180 deg [3]. The flame-spread limit for $0<\theta_1<180$ deg. is slightly inside FSL2, but is slightly outside FSL2 for $\theta_1=180$ deg. and $-45<\theta_1<0$ deg[3]. This suggests that Droplet C affects the flame-spread limit slightly. In the case of **Fig. 3(d)**, the flame-spread limits for $\theta_1=0$ and 90 deg. almost coincide with FSL2 of Droplets B and A or are slightly inside FSL2 considering the results in **Fig. 3(a)**. The results in the region of $\theta_1=-90$ deg. and $-90<\theta_1<-45$ deg. suggest that Droplet C affects the flame-spread limit because there is the flame-spreading condition outside FSL2 of Droplets B and A although Droplet L is outside FSL1 of Droplet C. Therefore, the pre-heating of Droplet L by the burning of Droplet C enlarges the flame-spread limit from interactive Droplets B and A.

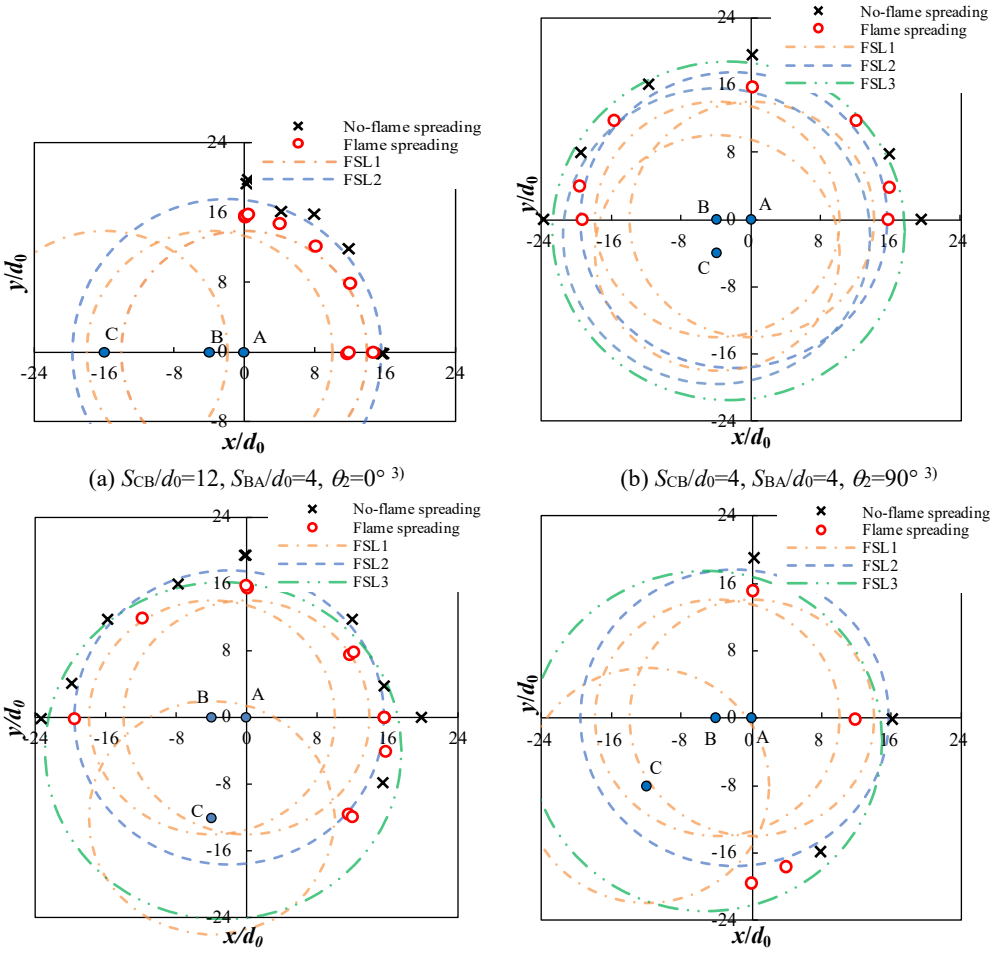

(a) $S_{CB}/d_0=12$, $S_{BA}/d_0=4$, $\theta_2=0°$ [3]

(b) $S_{CB}/d_0=4$, $S_{BA}/d_0=4$, $\theta_2=90°$ [3]

(c) $S_{CB}/d_0=12$, $S_{BA}/d_0=4$, $\theta_2=90°$ [3]

(d) $S_{CB}/d_0=11.3$, $S_{BA}/d_0=4$, $\theta_2=45°$

Fig. 3 Flame-spread-limit distribution for $S_{BA}/d_0=4$, where $S_{CB}/d_0=4$, 11.3, 12 and $\theta_2=0$ to 90 deg. The flame-spread-limit distance around single Droplet A is shown as a chain line. The flame-spread-limit distance around an imaginary droplet with twice the volume located at the center of the mass of Droplets B and A is shown as a dashed line and an imaginary droplet with three times the volume located at the center of the mass of Droplets C, B and A is shown as a two-dot chain line.

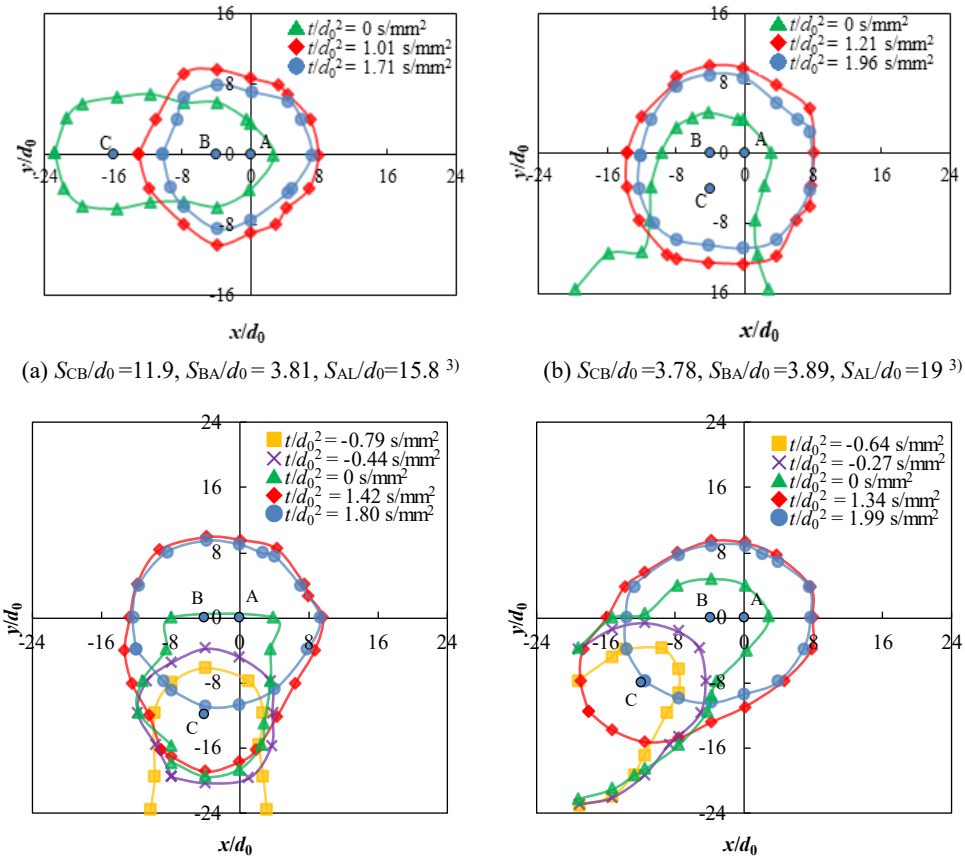

(a) S_{CB}/d_0 =11.9, S_{BA}/d_0 = 3.81, S_{AL}/d_0=15.8 [3)]

(b) S_{CB}/d_0 =3.78, S_{BA}/d_0 =3.89, S_{AL}/d_0 =19 [3)]

(c) S_{CB}/d_0 = 11.7, S_{BA}/d_0 =3.60, S_{AL}/d_0=19.7

(d) S_{CB}/d_0 =10.5, S_{BA}/d_0=3.70, S_{AL}/d_0 =19.5

Fig. 4 Iso-thermal line distributions of 1200 K during the flame spread in the case without flame spreading to Droplet L.

Figure 4 shows the iso-thermal line distribution according to the high-temperature region of the 14-μm SiC fiber at 1200 K obtained by the TFP method during the flame spread in the case without flame spreading to Droplet L. □ indicates the ignition time of Droplet C, ▵ indicates the ignition time of Droplet A, ♢ indicates the time of the maximum high-temperature region, and ○ indicates the time after a certain time from ♢.

Focusing on the iso-thermal line of ♢ where the high-temperature region is maximum, **Figs. 4(a)** and **(b)** show that it centers near the center of mass of interactive Droplets B and A and the interactive Droplets C, B and A, respectively. In the case of strong interaction by two or three interactive droplets, the high-temperature region is enlarged by droplet interaction in a circular shape at the center of the mass of the interactive droplets [3)]. In **Figs. 4(c)** and **(d)**, the high-temperature region expands in an elliptical shape around Droplets C, B, and A, and the burning of Droplet C ends after the high-temperature region becomes maximum. Then, interactive combustion occurs only with Droplets B and A, and the high-temperature region becomes nearly circular. In the case of **Fig. 4(a)**, at the time when the high-temperature region is maximum, the effects of Droplet C are almost eliminated, and the effect of the combustion of Droplets B and A is dominant. In the case of **Figs. 3(c)** and **(d)**, however, the effect of the burning of Droplet C is seen even at the time when the high temperature region is maximum, and in the case when Droplet L is positioned around Droplet C, it affects the flame spread to Droplet L.

Figure 5 shows the iso-thermal line distributions according to the high-temperature region at 1200 K in the case with flame spreading to Droplet L near the flame-spread limit. □, ▵ and ○ show the same time as in **Fig. 4**, + indicates the time when Droplet L is ignited. In the cases of **Figs. 5(a)**, **(b)**, **(g)** and **(h)**, according to the line perpendicular to the iso-thermal line at the time immediately before Droplet L was ignited, the ignition of Droplet L is most affected by the burning of Droplet A. In the case of **Fig. 5(c)**, the perpendicular line at the time when Droplet L was ignited is slightly extended from Droplet B, and therefore the ignition of Droplet L is most affected by the burning of Droplet B. In the case of **Fig. 5(d)**, according to the perpendicular line immediately before the ignition of Droplet L, the ignition of Droplet L is most affected by Droplet A.

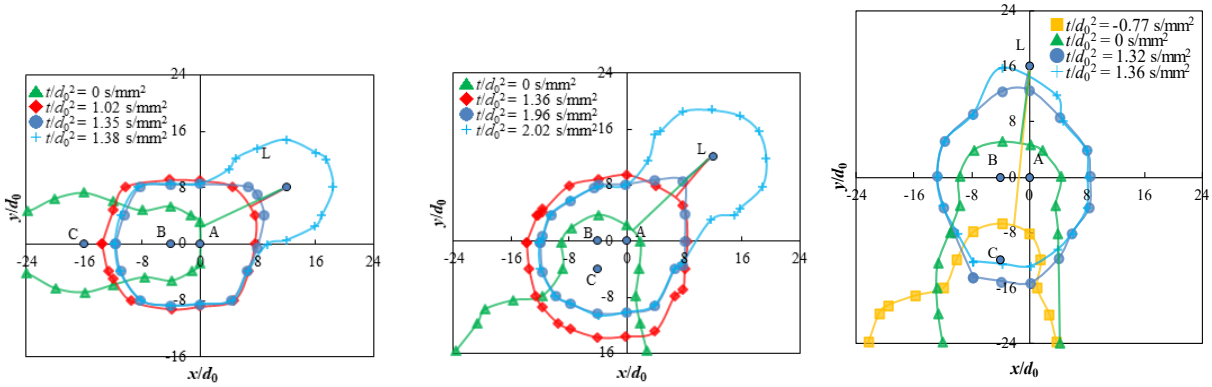

(a) S_{CB}/d_0=11.9, S_{BA}/d_0=4.01, S_{AL}/d_0=14.3 [3] (b) S_{CB}/d_0=3.87, S_{BA}/d_0=3.85, S_{AL}/d_0=16.6 [3] (c) S_{CB}/d_0=11.7, S_{BA}/d_0=3.82, S_{AL}/d_0=15.8

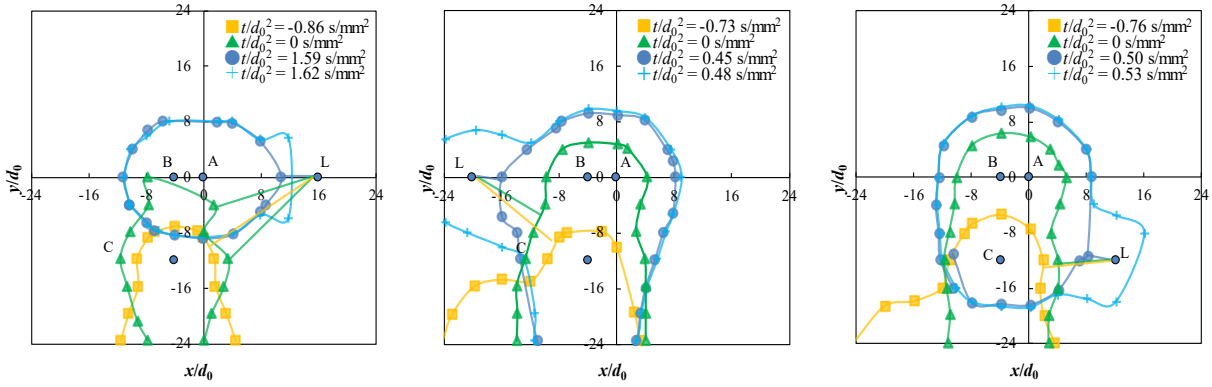

(d) S_{CB}/d_0=11.9, S_{BA}/d_0=3.74, S_{AL}/d_0=15.8 (e) S_{CB}/d_0=11.7, S_{BA}/d_0=4.02, S_{AL}/d_0=19.6 (f) S_{CB}/d_0=11.7, S_{BA}/d_0=3.97, S_{AL}/d_0=16.8

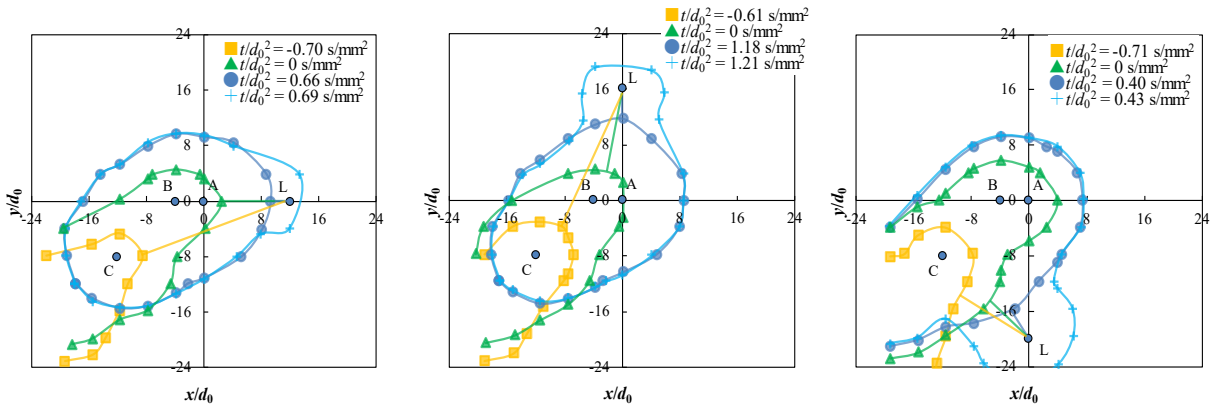

(g) S_{CB}/d_0=10.8, S_{BA}/d_0=3.66, S_{AL}/d_0=12.2 (h) S_{CB}/d_0=10.4, S_{BA}/d_0=3.89, S_{AL}/d_0=15.7 (i) S_{CB}/d_0=10.9, S_{BA}/d_0=3.86, S_{AL}/d_0=19.7

Fig. 5 Iso-thermal line distributions of 1200 K during the flame spread in the case with flame spreading to Droplet L near the flame-spread limit.

Focusing on the perpendicular line at the earlier time, the burning of Droplet C also has a strong effect. In the cases of **Figs. 5(e)**, **(f)**, and **(i)**, the burning of Droplet C most affected the ignition of Droplet L because the perpendicular line at each time extends from Droplet C to Droplet L. Since the flame around Droplet C preheated Droplet L from the outside of the flame-spread limit, it is considered that Droplet L outside the FSL2 of Droplets B and A was ignited thereafter. In the case with strong interaction in the closest arrangement of Droplets B and A, Droplet C affects the flame spread to Droplet L existing around Droplet C with θ_2=45 deg. and 90 deg. In addition, although experiments have not been performed under the condition that Droplet C is placed at θ_2=0 deg., if the flame spread experiment is conducted under the condition of 90

$<\theta_1<180$ deg., Droplet L would be expected to be affected by the burning of Droplet C and the flame-spread limit to be expanded.

4. Conclusions

We conducted microgravity experiments aboard Kibo on the ISS and performed a temperature-field analysis using the Thin Filament Pyrometry (TFP) method based on visible light emissions to study the effect of droplet interaction on the flame spread characteristics. We investigated the influence of the position of the interactive droplets on the flame spread considering temporal variation of the iso-thermal line distribution for droplet-cloud elements composed of four droplets, Droplets C, B and A of interactive droplets and Droplet L for confirmation of the flame spread. The position of Droplet L was varied to investigate the flame-spread limit from burning Droplet A to Droplet L. The direction angle θ_1 of Droplet L from the center line of Droplets B and A ranged from -90 deg. to 180 deg. The position of Droplet C was varied to investigate the effect of the position of the interactive droplet on the flame spread. The direction angle θ_2 of Droplet C from the center line of Droplets B and A was 0, 45 and 90 deg. Under a strong three-droplet interaction condition, such as the dimensionless droplet spacings between Droplets C and B and Droplets B and A of 4, the flame-spread limit extends greatly by the three droplet interaction. Under the condition with strong two-droplet interaction between Droplets B and A, Droplet C with dimensionless droplet spacing between Droplets C and B of 12, which has no significant interaction, the burning of Droplet C with θ_2=90 deg. slightly increases the flame-spread limit even for θ_1=0 deg. and 180 deg. The flame-spread limit around θ_1=-45 deg. is also extended by the burning of Droplet C through the pre-vaporization of Droplet L existing outside the flame-spread limit of Droplet C and being preheated by the burning of Droplet C.

Acknowledgments

This research was conducted as the "Group Combustion" project by JAXA and was subsidized by JSPS KAKENHI Grant-in-Aid for Scientific Research (B) (18H01625) and JSPS KAKENHI Grant-in-Aid for JSPS Research Fellow (18J15253).

References

1) M. Mikami, M. Kikuchi, Y. Kan, T. Seo, H. Nomura, Y. Suganuma, O. Moriue and D.L. Dietrich: Int. J. Microgravity Sci. Appl., **33** (2016) 330208.
2) M. Mikami, Y. Yoshida, T. Seo, T. Sakashita, M. Kikuchi, T. Suzuki and M. Nokura: Microgravity Sci. Technol., **30** (2018) 535.
3) Y. Yoshida, K. Iwai, K. Nagata, T. Seo, M. Mikami, O. Moriue, T. Sakashita, M. Kikuchi, T. Suzuki and M. Nokura: Proc. Combust. Inst., **37** (2019) 3409.
4) M. Kikuchi, Y. Kan, A. Tazaki, S. Yamamoto, M. Nokura, N. Hanafusa, Y. Hisashi, O. Moriue, H. Nomura and M. Mikami: Trans. JSASS Aerospace Tech. Japan, **12** (2014) No. ists29, Th_25-Th_30.
5) M. Mikami, H. Oyagi, N. Kojima, M. Kikuchi, Y. Wakashima and S. Yoda: Combust. Flame, **141** (2005) 241.
6) T. Farouk, and F.L. Dryer: Combustion Theory and Modelling, **15** (2011) 487.
7) H. Oyagi, H. Shigeno, M. Mikami and N. Kojima: Combust. Flame, **156** (2009) 763.
8) M. Mikami, H. Nomura, Y. Suganuma, M. Kikuchi, T. Suzuki and M. Nokura: Int. J. Microgravity Sci. Appl., **35** (2018) 350202.
9) M. Mikami, H. Watari, T. Hirose, T. Seo, H. Saputro, O. Moriue and M. Kikuchi: J. Thermal Sci. Technol., **12** (2017) JTST0028.